

1 **Heterologous Expression of *Pseudomonas putida* Methyl-Accepting Chemotaxis**

2 **Proteins Yields *Escherichia coli* Chemotactic to Aromatic Compounds**

3

4 Clémence Roggo^{1#}, Estelle Emilie Clerc^{1,2}, Noushin Hadadi¹, Nicolas Carraro¹, Roman

5 Stocker², and Jan Roelof van der Meer^{1*}

6

7 1) Department of Fundamental Microbiology, University of Lausanne, 1015 Lausanne,
8 Switzerland

9 2) Institute for Environmental Engineering, ETH Zürich, 8093 Zürich, Switzerland

10

11

12

13 *Corresponding author

14 J. R. van der Meer

15 Department of Fundamental Microbiology

16 Bâtiment Biophore

17 Quartier UNIL-Sorge

18 University of Lausanne

19 1015 Lausanne

20 Switzerland

21

22 Email: janroelof.vandermeer@unil.ch

23

24 #Present address:

25 University of Applied Sciences and Arts, Western Switzerland, Changins, 1260 Nyon

26

27

28

29 Running title: *Escherichia coli* chemotactic to aromatic compounds

30 **ABSTRACT (250 w.)**

31 *Escherichia coli*, commonly used in chemotaxis studies, is attracted mostly by amino acids,
32 sugars and peptides. We envisioned modifying chemotaxis specificity of *E. coli* by expressing
33 heterologous chemoreceptors from *Pseudomonas putida* enabling attraction either to toluene
34 or benzoate. The *mcpT* gene encoding the type 40H methyl-accepting chemoreceptor for
35 toluene from *Pseudomonas putida* MT53 and the *pcaY* gene for the type 40H receptor for
36 benzoate and related molecules from *P. putida* F1 were expressed from the *trg* promoter on a
37 plasmid in motile wild-type *E. coli* MG1655. *E. coli* cells expressing McpT accumulated in
38 chemoattraction assays to sources with 60–200 μ M toluene; less strongly than the response to
39 100 μ M serine, but statistically significantly stronger than to sources without any added
40 attractant. An McpT-mCherry fusion protein was detectably expressed in *E. coli* and yielding
41 weak but distinguishable membrane and polar foci in 1% of cells. *E. coli* expressing PcaY
42 showed weak attraction to 0.1–1 mM benzoate but 50–70% of cells localized the PcaY-
43 mCherry fusion to their membrane. We conclude that implementing heterologous receptors in
44 the *E. coli* chemotaxis network is possible and, upon improvement of the compatibility of the
45 type 40H chemoreceptors, may bear interest for biosensing .

46

47 **IMPORTANCE (150 w.)**

48 Bacterial chemotaxis might be harnessed for the development of rapid biosensors, in which
49 chemical availability is deduced from cell accumulation to chemoattractants over time.
50 Chemotaxis of *Escherichia coli* has been well-studied, but the bacterium is not attracted to
51 chemicals of environmental concern, such as aromatic solvents. We show here that
52 heterologous chemoreceptors for aromatic compounds from *Pseudomonas putida* at least
53 partly functionally complement the *E. coli* chemotaxis network, yielding cells attracted to
54 toluene or benzoate. Complementation was still inferior to native chemoattractants like serine,
55 but our study demonstrates the potential for obtaining selective sensing for aromatic
56 compounds in *E. coli*.

57

58 INTRODUCTION

59

60 Chemotaxis is a rapid (second-scale) behavior of motile organisms to swim towards an
61 attractant or away from a repellent. Chemotactic bacteria can produce a variety of
62 chemoreceptors, some of which with high chemical specificity and selectivity, and others
63 reacting more broadly to related compound classes (1). Chemotaxis could thus be an
64 interesting property for the development of bacterial-based biosensors, which might
65 eventually be deployed to detect and quantify chemical targets in samples (2, 3).

66 Chemotaxis of *Escherichia coli* is strong and highly reproducible with known and
67 potent chemoattractants, such as serine or aspartate, and has been widely studied (4, 5).
68 Unfortunately, *E. coli* does not naturally display chemotaxis towards molecules of potential
69 interest for environmental monitoring, such as aromatic or chlorinated solvents. Given its
70 relatively narrow native chemo-attractant range, it is interesting to investigate whether the *E.*
71 *coli* chemotaxis system can be complemented by heterologous chemoreceptors. One
72 important characteristic of methyl-accepting chemotaxis proteins (MCPs) and chemotaxis
73 effector proteins (e.g., CheY) is their structural conservation among bacteria (6-8). *E. coli*
74 possesses five chemotaxis receptors, but other environmental bacteria frequently encode
75 many more chemoreceptors albeit with often unknown effectors. For example, *Pseudomonas*
76 species can encode more than 20 MCPs in their genomes (9, 10). A few studies have
77 demonstrated successful expression of heterologous chemoreceptors in *E. coli*. For example,
78 several MCPs from *Shewanella oneidensis* could be expressed in *E. coli*, enabling energy
79 taxis with nitrate (11). Also, Aer-2, a soluble receptor from *Pseudomonas aeruginosa*
80 involved in aerotaxis, and PctApp, a putative MCP for amino acids from *Pseudomonas putida*
81 were shown to partially trigger chemotaxis response when expressed in *E. coli* (12, 13).
82 However, no MCPs involved in sensing of environmental pollutants have to date been
83 functionally expressed in *E. coli*.

84 As part of the characterization of bacterial biodegradation pathways, several bacteria

85 were shown to be chemotactic to aromatic compounds, such as to naphthalene, toluene,
86 benzoate or 2,4-dichlorophenoxyacetic acid (14-17). Some bacteria have been characterized
87 in some detail as to their MCPs and chemical effector(s). For example, an MCP named McpT
88 was identified on the self-transmissible plasmid pCRT1 in *P. putida* DOT-T1E, which
89 enables chemotaxis to toluene and naphthalene (18, 19). This *mcpT* gene may be more
90 widespread among pseudomonads, as it possesses 99.8% sequence similarity to coding
91 sequences on the TOL plasmid pWW53 of *P. putida* MT53 (19). Strain MT53 was mentioned
92 as a moderate chemotactic responder to toluene. Further chemoreceptors have been
93 characterized in *P. putida* F1. As an example, the PcaY receptor was shown to be involved in
94 chemotaxis towards vanillate, vanillin, 4-hydroxybenzoate, benzoate, protocatechuate,
95 quinate and shikimate (20).

96 The primary goal of this work was to investigate whether chemotaxis specificity of *E.*
97 *coli* could be expanded towards aromatic compounds. This could be used as proof of concept
98 for the future development of biosensing strains of *E. coli*, selectively chemotactic towards
99 environmental pollutants, for deployment in quantitative biosensor microfluidic platforms (3).
100 Our strategy was to express the *mcpT* gene from *P. putida* MT53 (pWW53) or the *pcaY* gene
101 from *P. putida* F1 on a selectable plasmid in motile *E. coli* wild-type MG1655 and in a
102 mutant background in which the gene for the major chemoreceptor Tsr was deleted, and to
103 compare chemotaxis to toluene or benzoate with chemotaxis to serine or to no attractant in
104 strains expressing or not the *mcpT* or *pcaY* gene. Compound-specific chemotaxis was
105 quantified in two manners: firstly, by microscopy and image analysis from cell accumulation
106 nearby solid agarose sources containing the respective chemo-attractant; and secondly, by a
107 recently developed in-situ chemotaxis microfluidic assay (ISCA) (21). Subcellular
108 localization of the heterologous MCP receptors was assessed and quantified from expressed
109 equivalent mCherry-fusion proteins in *E. coli* observed by epifluorescence microscopy, in
110 comparison to that of a Tsr-mCherry fusion.

111

112 RESULTS

113

114 **Chemotactic response of *E. coli* to attractants in agarose plug assays.** In order to
115 quantify *E. coli* chemotaxis to different molecules, we used two independent assays:
116 microscopy observation of cell accumulation to chemoattractants diffusing from a solid
117 agarose source, and a microfabricated *in situ* chemotaxis assay (ISCA). The agarose plug
118 assays in microscope settings (22) embeds the test compound in a solidified cylinder (\varnothing 4 mm,
119 height 0.15 mm) of agarose (the *source*), while introducing a homogenous *E. coli* cell
120 suspension in motility buffer around the source (Fig. S1 in the Supplemental Material). The
121 bacteria accumulation nearby the source edge was recorded by phase-contrast microscopy
122 after 15 min incubation at 21°C and quantified using image analysis (Fig. S1). Robust
123 chemotaxis of *E. coli* MG1655 was detected to the known chemoattractants serine, aspartate
124 and methylaspartate at 10 and 100 μ M source concentration (Fig. 1A, B). In contrast, cell
125 accumulation of *E. coli* MG1655 to the weaker chemoattractants ribose or galactose at 10 or
126 100 μ M was not statistically significantly different from cells accumulating on the edge of
127 agarose sources without any attractant added (Fig. 1C). These results indicate that the agarose
128 plug assay protocol can be used to measure *E. coli* attraction to chemical targets with a
129 'strength of attraction' in between ribose/galactose and serine/aspartate/methylaspartate.

130 **Chemotaxis of *E. coli* expressing the McpT protein of *P. putida*.** Chemotaxis to
131 toluene was tested in motile *E. coli* MG1655 expressing the *mcpT* gene from plasmid pWW53
132 of *P. putida* MT53 (23) on plasmid pSTV28. In first instance, the *mcpT* gene was expressed
133 from the low constitutive synthetic P_{AA} promoter (24), but this yielded only few viable
134 transformants that always contained mutations in *mcpT*, causing frameshifts leading to a
135 premature stop codon or a deletion. In contrast, expression of the *mcpT* gene on plasmid
136 pSTV28 from the *trg* promoter (also controlling transcription of the native Trg chemoreceptor
137 in *E. coli* (25)), resulted in many viable transformants with correct sequences of *mcpT*. This
138 indicated that we could achieve expression of McpT in *E. coli* using the *trg* promoter.

139 Observing attraction to toluene is complicated by the technical difficulties to produce
140 a solid source containing toluene, which is poorly soluble in water and volatile. First attempts
141 using toluene dissolved in eicosane or dimethylsulfoxide before mixing with agarose were
142 unsuccessful. We could improve consistency by mixing small volumes of liquid toluene
143 directly with dissolved agarose at 55°C inside completely filled and closed glass vials. Indeed,
144 *E. coli* cells expressing McpT from the *trg* promoter on plasmid pCRO20 incubated in
145 motility buffer accumulated close to a solid agarose source with a 10⁻³ toluene dilution
146 (equivalent to 60 µM, Fig. 2A, B). Accumulation of cells in response to toluene was less
147 pronounced than in response to a 100 µM serine source but statistically significantly higher
148 than with sources without any attractant added (Fig. 2A, B, one-way ANOVA and multiple
149 comparison, p=0.0119). Accumulation was robust across fourfold replicates and experiments
150 carried out independently on different days (Fig. 2B). The variation in the magnitude of
151 accumulation was more important with toluene (±31% of the average) than with serine (±3%,
152 Fig. 2B inset), which is likely due to the variation in preparing consistent sources with a
153 volatile attractant. At a tenfold lower toluene source concentration (6 µM), cell accumulation
154 of *E. coli* pCRO20 at the source edge was no different than to a source without anything
155 added (Fig. 2B, inset). A tenfold higher source concentration of toluene (600 µM) did not
156 result in cells accumulating near the source surface, even though the cells were visibly still
157 motile and able to swim in the proximity of the source (data not shown).

158 In contrast to *E. coli* expressing McpT, cells of both *E. coli* containing the empty
159 plasmid pSTV28 and *E. coli* carrying a plasmid with a frameshift mutation in the *mcpT*
160 coding sequence causing premature ending (pCRO35) did not accumulate towards a 60 µM
161 toluene source to a higher degree than to a source without attractant added (Fig. 2C, D and
162 Fig. S2). Both strains, however, responded as expected to a 100 µM serine source and thus
163 were chemotactic (Fig. 2C, D).

164 **Chemotactic response of *E. coli* expressing the PcaY receptor for benzoate.** In
165 separate experiments, we expressed in motile *E. coli* MG1655 the gene for the PcaY receptor
166 from *P. putida* F1, which has been reported to induce chemotaxis to molecules such as

167 vanillate, vanillin, 4-hydroxybenzoate, benzoate, protocatechuate, quinate and shikimate (20).
168 Cells of *E. coli* MG1655 (pCRO33) expressing PcaY from the *trg* promoter accumulated
169 nearby a source plug with 1 mM benzoate. The response was weaker than the response to 100
170 μ M serine but stronger than to a source without added attractant (Fig. 3A). A lower
171 concentration of benzoate (0.1 mM) decreased cell accumulation to a level no different from
172 that observed without attractant added (Fig. 3A). Cells of *E. coli* MG1655 pSTV28 (without
173 *pcaY*) also accumulated nearby a 1 mM benzoate source, with similar intensity to MG1655
174 (pCRO33) (Fig. 3B). Cell accumulation of *E. coli* MG1655 (pCRO33) to sources of 4-
175 hydroxybenzoate and vanillate (at 0.1 and 1 mM) was not significantly different than to a
176 source without attractant added.

177 **Chemotactic cell accumulation in microfabricated wells.** As a second independent
178 method for chemotaxis quantification we deployed the recently developed ISCA assay (21).
179 The ISCA consists of five replicates of \sim 110- μ l wells, fabricated out of the biocompatible
180 polymer polydimethylsiloxane (PDMS) bonded to a glass slide. The wells are filled with a
181 chemoattractant solution and then immersed in a dilute cell suspension ($2\text{--}4 \times 10^6$ cells ml^{-1}).
182 A single acentrically placed port (\varnothing 0.8 mm) functions as inlet channel, through which the
183 chemoattractants diffuse out to form gradients and through which motile, chemotactically
184 attracted cells can enter into the wells. Washed *E. coli* MG1655 wild-type motile cells
185 suspended in motility buffer (strain 4498) accumulated up to five-fold inside the ISCA
186 cavities within a 35-min incubation period with 100 or 300 μ M serine as chemoattractant, in
187 comparison to motility buffer (MB) alone (Fig. 4A). In contrast, cells did not statistically
188 significantly accumulate to benzoate at 100 or 300 μ M concentrations in comparison to MB,
189 but were statistically significantly repelled at higher benzoate concentrations (300 and 1000
190 μ M) and by toluene at 60 and 200 μ M dosages (Fig. 4A). *E. coli* MG1655 cells expressing
191 the McpT receptor (plasmid pCRO20, strain 5197) consistently accumulated inside ISCA
192 wells filled with serine (100 and 300 μ M), as well as with toluene at 60 and 200 μ M (\sim 3-
193 fold), but not with benzoate (300 μ M), in comparison to MB (Fig. 4B). Cells were not
194 attracted to a higher concentration of toluene (600 μ M, Fig. 4B). *E. coli* MG1655 cells

195 expressing PcaY from plasmid pCRO33 (strain 5447) were attracted to serine, as expected,
196 and slightly (1.2-fold) to 300 μ M benzoate, although this was not statistically significant from
197 MB alone (Fig. 4C) as a result of larger variation across replicates. Strain 5447 cells were
198 repelled by high benzoate concentrations, but not by toluene (Fig. 4C). However, in an *E. coli*
199 MG1655 motile background in which the major chemoreceptor Tsr (for serine) was deleted
200 and PcaY was expressed, accumulation to serine was largely absent, and a statistically
201 significant response to benzoate was observed (1.5-fold; Fig. 4D). Expression of McpT from
202 plasmid pCRO20 in the *E. coli* Δ *tsr* background yielded cells no longer accumulating to
203 serine, but attraction to toluene did not further improve (1.7-times accumulation at a 200 μ M
204 toluene dosage, Fig. 4E).

205 **Localization of the expressed *P. putida* MCPs in *E. coli*.** In order to further
206 demonstrate whether McpT and PcaY are functionally produced in *E. coli*, their coding
207 regions were translationally fused with that for mCherry (without start codon itself). The
208 fusion genes were cloned and again expressed under the *trg* promoter on plasmid pSTV28
209 (Fig. S2 and S3) in either *E. coli* MG1655 motile wild-type or the Δ *tsr* deletion background.
210 As a positive control, we used *E. coli* MG1655 cells expressing a Tsr-mCherry fusion protein
211 from the *trg* promoter on plasmid pSTV28. These cells showed bright fluorescence, which
212 was enriched in the membrane and in broad zones near the cell poles (Fig. 5B). An *E. coli*
213 control expressing Tsr alone (without mCherry) was not fluorescent (Fig. 5A). Projection of
214 detectable foci (see *Materials and Methods* for ‘foci’ detection) as well as overall pixel
215 intensities across all imaged cells normalized to a standardized *E. coli* cell length as in Figure
216 6A and 6B showed the strong overall polar localization of Tsr-mCherry fusion protein. This is
217 in agreement with previous studies and what is expected for the localization of the major *E.*
218 *coli* chemoreceptors (26, 27). *E. coli* cells expressing McpT-mCherry were on average more
219 fluorescent than *E. coli* MG1655, MG1655 expressing McpT alone (without mCherry), or
220 MG1655 expressing a frameshifted *mcpT-mCherry* (Fig. 5C-E, note fluorescence scales). A
221 small proportion of cells (~1%) contained confined (but rather weak) fluorescent foci in the
222 membrane (Fig. 5C, arrows). Superposed projection of all detected fluorescent foci across

223 imaged cells showed that McpT-mCherry expression was localized in the membrane area of
224 the cells and the poles (Fig. 6A). Cells expressing truncated McpT-mCherry still displayed
225 some fluorescence, which might be the result of a start codon downstream the frameshift
226 position in *mcpT*, but never produced any visible foci (Fig. 5D). Projection of detected foci
227 produced very few and spurious spots across many cells of both *E. coli* expressing McpT
228 without mCherry fusion or the frame-shifted McpT-mCherry (Fig. 6A). Enrichment of McpT-
229 mCherry foci near the cell poles was clearer in an *E. coli* Δ *tsr* background (Fig. 6A). We
230 further quantified mCherry-fusion protein expression by recording the mean intensity of the
231 top-10% brightest pixels per cell, normalized to the mean fluorescent brightness over all
232 individual cells (Fig. 6C). Mean top-10% fluorescence was statistically significantly higher in
233 *E. coli* wild-type and Δ *tsr* background expressing McpT-mCherry than in *E. coli* expressing
234 McpT or the frame-shifted McpT-mCherry (Fig. 6C).

235 *E. coli* expressing *pcaY-mCherry* showed on average brighter fluorescence
236 localization in the cellular membrane and frequently at the cell poles (Fig. 5F, 6A), in a higher
237 proportion of cells (50-70%), and the top-10% fluorescence was clearly higher than *E. coli*
238 expressing McpT-mCherry (Fig. 6C). Fluorescence of the expressed PcaY-mCherry was less
239 bright than in case of Tsr-mCherry (Fig. 5B, 6C), but its localisation was similar (Fig. 6A).
240 Expression of PcaY-mCherry in a Δ *tsr* background increased the top-10% fluorescence level
241 of cells, suggesting higher expression and or more appropriate oligomerization.

242 These results thus confirmed that the McpT- and PcaY-mCherry receptors are
243 expressed in *E. coli* and are preferentially localised to the cell membrane and poles. In
244 contrast to expression of Tsr- and PcaY-mCherry, the proportion of *E. coli* cells with visibly
245 localised McpT- mCherry fluorescence was low (~1%).

246

247 **DISCUSSION**

248 Heterologous expression of chemoreceptors and functional complementation of chemotaxis in
249 *E. coli* is not straightforward, and relatively few studies have examined it (11, 13). The major
250 aim of this work was to investigate the possibility to functionally express chemoreceptors for

251 detection of aromatic compounds from *P. putida* in motile *E. coli*. We focused on two
252 chemoreceptors, McpT (18, 19) and PcaY (20), which from studies in their native host or by
253 analogy, were reported to detect and signal the presence of toluene and benzoate (plus a
254 further range of substituted aromatic compounds), respectively. By using two different
255 chemotaxis assays and by studying expression and subcellular localisation of chemoreceptor-
256 mCherry fusion proteins, we conclude that both chemoreceptors are functionally expressed in
257 *E. coli* and can lead to chemotaxis of motile *E. coli* towards toluene or benzoate at source
258 concentrations in the range of 60–300 μ M. Accumulation was concentration dependent,
259 which is a hallmark of chemotaxis. But the range of source concentrations yielding
260 measurable cell accumulation was relatively narrow, which may be due to toxicity or
261 repellent-response at higher chemoattractant concentrations.

262 Chemotaxis of *E. coli* expressing the heterologous chemoreceptors McpT or PcaY is
263 relatively weak compared to its major chemoattractant serine. This may be due to the small
264 proportion of cells correctly expressing and localising the McpT or PcaY chemoreceptors
265 (Fig. 6A–H), and to a general poor compatibility of this class of chemoreceptors with *E. coli*
266 downstream signaling proteins CheA and CheW. According to the chemoreceptor
267 classification of Alexander et al. (6), McpT and PcaY belong to the 40-helical bundle (40H)
268 type, whereas the *E. coli* MCPs (like Tsr and Tar) are part of the 36H type. Although the two
269 chemoreceptor types have strong sequence conservation in the signaling domain (Fig. S4),
270 with conserved amino acids at positions known to be contacted by CheA and CheW (28),
271 notably the positions of methylation sites are partly different or absent in the 40H-type, and
272 also the nature of the residue for inter-dimer trimerization of Tsr (Phe-373) is charged instead
273 of hydrophobic in the 40H-type (6). The consequence of this may be different oligomerization
274 arrangements of expressed 40H-type chemoreceptors in *E. coli* and poorer downstream
275 signaling.

276 Despite this, detectable fluorescent foci and fluorescent membrane zones in *E. coli*
277 cells (Fig. 6) indicated that McpT-mCherry and PcaY-mCherry are mostly localized in the
278 membrane and cell poles. Expression of McpT- and PcaY-mCherry was much weaker than

279 that of Tsr-mCherry expressed from the same *trg* promoter on plasmid pSTV, even in an *E.*
280 *coli* host devoid of Tsr, although the average top–10% pixel fluorescence further increased in
281 *E. coli* Δ *tsr* compared to wild-type (pCRO33) with *pcaY-mCherry* (Fig. 6C). When assuming
282 that the localisation of McpT and PcaY is analogous to their -mCherry counterparts, these
283 results are a further sign that their folding or membrane oligomerization is not optimal for *E.*
284 *coli*. The relatively small proportion of cells with visible McpT-mCherry foci (~1%, Fig. 5C)
285 might be an indication that only a small subpopulation of *E. coli* actually is responsive to
286 toluene, which would explain the relatively poor overall accumulation of motile cells in
287 suspensions. Our results are thus in agreement with previous studies demonstrating successful
288 heterologous expression in *E. coli* of other non-native type 40H–receptors, such as the PctA
289 serine-receptor of *P. putida* (13) or the nitrate energy-taxis MCPs from *S. oneidensis* (11).
290 Expression of the PctA receptor from a salicylate-inducible system yielded at least partially
291 properly protein-protein interactions to *E. coli* CheA and CheY, although cell accumulation
292 was only observed at 10 mM serine (13). Type 40H chemoreceptors thus seem to connect to
293 the *E. coli* chemotaxis signaling pathways, but with lesser efficiency in attractant-biased
294 motility.

295 One of the issues when studying heterologous chemoreceptor expression in *E. coli*
296 and its correspondingly weaker or different chemotactic behaviour, is the poor sensitivity and
297 reproducibility of most traditional chemotaxis assays, such as capillary assays, swimming
298 plates or source accumulation assays. We showed here how cell accumulation to
299 chemoattractants at concentrations of the order of 100 μ M concentrations can be more
300 accurately quantified from microscopic agarose plug assays with standard errors in the order
301 of 5% of the mean (Fig. 1). Cell accumulation in the wells of the ISCA device across five
302 replicates was slightly more variable (standard error ~15% of the mean), which is most likely
303 due to the lower concentration of cells used ($2\text{--}4 \times 10^6$ versus 10^9 cells ml^{-1}), or, possibly, to
304 small differences in the geometry of the wells or fluid motion while incubating the cell
305 suspension. We noted additional effects on the outcome of the ISCA assays related different
306 growth temperatures of the *E. coli* culture (30°C or 37°C), the cell treatment procedure

307 (washing in motility buffer or not), and assay incubation temperature (preheating culture
308 media). ISCA assays confirmed previous studies that benzoate is a repellent for *E. coli* and
309 *Salmonella* (29), but only at concentrations above 300 μM (Fig. 4). Toluene acts as repellent
310 for wild-type *E. coli* MG1655 already in the range of 60–200 μM (Fig. 4A). At lower
311 benzoate concentrations *E. coli* MG1655 chemotaxis is not significantly perturbed, and cells
312 expressing the PcaY receptor showed a net positive attraction to 300 μM benzoate (1.5–2.0
313 fold when compared to accumulation of *E. coli* MG1655 on 300 μM benzoate).

314 We conclude, albeit carefully, that the *E. coli* chemoattractant repertoire can be
315 expanded to aromatic compounds by heterologous expression of *P. putida* type 40H
316 chemoreceptors. It could potentially be interesting to use *E. coli* chemotaxis for quantitative
317 sensing of chemicals, because of the relatively rapid response time (5–30 min in microfluidic
318 assays, Ref. (3)) and its potentially narrower detection selectivity than the original host
319 bacteria. For instance, *P. putida* encodes 20 potential chemoreceptors with partially
320 overlapping chemoattractants (9, 10) compared to *E. coli* with only five. Quantification of cell
321 accumulation as a function of chemoattractant concentration may further be improved by
322 using microfluidic platforms in which stable chemical gradients can be produced, as we have
323 recently shown (3). However, if heterologously expressed chemoreceptors in *E. coli* are to be
324 used for quantitative sensing of chemoattractants, their compatibility with the existing *E. coli*
325 chemotaxis machinery has to be improved. For that matter, an alternative and successful
326 approach recently showed that functional hybrid receptors can be expressed in *E. coli* by
327 fusing non-cognate ligand-binding domains to the signaling domain of its chemoreceptors.
328 Reactions to ligands can be measured by Förster–resonance energy transfer between CheY and
329 CheZ (30, 31). The existing *E. coli* chemotaxis machinery can thus be expanded both by
330 hybrid as well as heterologous chemoreceptors and could pave the way for future faster and
331 selective biosensors.

332

333 MATERIALS AND METHODS

334

335 **Cloning procedures.** The gene for the methyl-accepting chemotaxis receptor (*mcpT*)
336 was amplified from *P. putida* MT53 pWW53 (23) (Table 1) genomic DNA by using Q5
337 proofreading polymerase (New England Biolabs) and primers 141001 and 141002 (Table S1).
338 The forward primer 141001 contained a BamHI restriction site and the reverse primer 141002
339 was elongated with a ClaI restriction site. The PCR fragment was cloned into pGEM-t-Easy[®]
340 (Promega) and the insert was verified by sequencing (Fig. S3). The *trg* promoter of the *E. coli*
341 chemoreceptor gene for Trg was amplified from *E. coli* MG1655 genomic DNA using a Q5
342 proofreading polymerase and primers 150613, elongated with a BamHI site, and 150612, with
343 a SacI restriction site and including the 17-bp 5'-part of *mcpT* until its internal NheI site (Fig.
344 S3). The *trg* promoter fragment was inserted upstream of the *mcpT* sequence in pGEM-t-
345 Easy[®] by digestion with BamHI and NheI, taking advantage of *mcpT*-internal NheI site (Fig.
346 S2). The correct fragment was finally inserted into pSTV28 by digestion with SacI and ClaI,
347 and the plasmid was renamed pCRO20 (Table 1, Fig. S2, S3). This plasmid was inserted into
348 a verified motile strain of *E. coli* MG1655 (*E. coli* Genetic Center, Yale, CGSC#8237, Table
349 1).

350 A frameshift mutation was introduced in *mcpT* to disrupt its coding sequence, by
351 digestion of pCRO20 with NsiI, removal of the 3'-overhangs by treatment for 20 min at 12 °C
352 with T4 DNA polymerase (New England Biolabs), and recircularization of the plasmid with
353 T4 DNA ligase. After transformation, this plasmid was renamed pCRO35 (Table 1, Fig. S2).

354 A *mcpT-mcherry* fusion was produced by amplification of a '*linker-mcherry*' fragment from
355 plasmid pBAM-link-mcherry (32) using primers 170239 and 170240 elongated with a BglII
356 restriction site and the C-terminal part of *mcpT* until the internal MfeI site, respectively (Table
357 S1, Fig. S2). The '*link-mcherry*' fragment was inserted in pCRO20 by digestion with BglII
358 and MfeI. This plasmid was renamed pCRO36 (Table 1, Fig. S2).

359 The receptor gene for PcaY from *P. putida* F1 was also cloned under the control of
360 the *trg* promoter on pSTV28. Its coding sequence (*Pput2149*) was amplified from *P. putida*
361 F1 genomic DNA using primers 160306 and 160307, whereas the *trg* promoter was amplified
362 using primers 150613 and 160305 (Table S1). Both PCR fragments were fused by sewing

363 PCR and cloned back into pSTV28 by digestion with SacI and ClaI. This plasmid was
364 renamed pCRO33 (Table 1, Fig. S2). To fuse the *pcaY* with *mcherry* reading frame, pCRO33
365 was digested with ClaI and EcoRI and the backbone was recovered. The *trg*-promoter-*pcaY*
366 fragment was reamplified and combined with the '*link-mcherry*' fragment by sewing PCR,
367 using primers 170931 and 170932. This fragment was then reinserted into the pCRO33-ClaI-
368 EcoRI backbone using In-Fusion HD cloning (Takara).

369 The *tsr* coding sequence was amplified from *E. coli* MG1655 genomic DNA using
370 primer 160309 and 160310, whereas the *trg* promoter fragment was amplified using primers
371 150613 and 160308 (Table S1). Both fragments were fused by sewing PCR and subcloned
372 into pGEM-t-Easy[®]. The complete part was then recovered and introduced into pSTV28 by
373 digestion with SacI and PstI (localized in pGEM-t-Easy[®]). This plasmid was renamed
374 pCRO34 (Table 1).

375 A *tsr-mcherry* fusion was produced by amplification of the '*link-mcherry*' fragment
376 from pBAM-link-mcherry using primers 101003 and 101004, and a '*P_{trg}-tsr*' fragment from
377 pCRO34 using primers 070418 and 160308 (Table S1). Both fragments were fused by sewing
378 PCR, subcloned into pGEM-t-Easy[®] and cloned back into pCRO34 by digestion with SacI
379 and SpeI. This plasmid was named pCRO38 (Table 1). Relevant plasmids were then further
380 transformed into *E. coli* MG1655- Δ *tsr* (strain 5396) with a complete deletion of *tsr* by double
381 recombination.

382 **Preparation of *E. coli* cultures for chemoattraction assays.** *E. coli* strains were
383 grown overnight at 37°C with 180 rpm shaking in M9 minimal medium supplemented with 4
384 g l⁻¹ of glucose, 1 g l⁻¹ of Bacto[™] casamino acids (BD difco), Hutner's trace metals (33), 1
385 mM of MgSO₄ and 30 μg ml⁻¹ of chloramphenicol (hereafter called M9-Glc-Cm30). The
386 cultures were diluted 100-fold in the morning in fresh M9-Glc-Cm30 and incubated for 3 h at
387 37°C with 180 rpm shaking until they reached exponential phase (culture turbidity at 600 nm
388 of between 0.5 and 0.6). For chemoattraction assays, 1–5 milliliter of culture was centrifuged
389 at 2,400×g for 5 min, the upper 0.9 ml of liquid were carefully removed (note that motile cells
390 do not really sediment), and replenished with 1 mL of motility buffer (motility buffer is 10

391 mM potassium phosphate, 0.1 mM EDTA, 10 mM lactate, pH 7.0) (34). This procedure was
392 repeated once more and finally the cells were resuspended in 500 μl of motility buffer,
393 yielding a density of $\sim 10^9$ cells ml^{-1} .

394 For ISCA assays, 5 ml of washed exponentially growing culture in M9-Glc-Cm30
395 was diluted in 300 ml preheated (37°C) motility buffer to obtain a cell concentration of 2–4
396 $\times 10^6$ cells ml^{-1} , and this suspension was used within 30 min. Note that we kept the washing
397 procedure the same between both chemotaxis assays, although we noticed that directly
398 diluting exponentially growing cells in motility buffer (without any centrifugation) increases
399 the proportion of cells responsive to 100 and 300 μM serine in the ISCA assay by almost a
400 factor of ten. This did not measurably influence the cell accumulation to toluene and
401 benzoate.

402 **Preparation of the chemoattractant sources.** As positive control for *E. coli*
403 chemotaxis, 1.4 ml of 2% dissolved agarose (LE, Analytical grade, Promega) solution at 55°C
404 was supplemented with 0.15 ml of 1 mM serine solution in water (final serine concentration =
405 100 μM). The negative control consisted of 1.8% agarose solution in tap water. Further test
406 sources for *E. coli* consisted of aspartate, *N*-Methyl-D-aspartate, D-ribose and D-Galactose
407 with final concentrations of 10 and 100 μM .

408 To prepare the source of toluene, 1.8 % of agarose was dissolved in tap water and
409 kept at 55°C . 2 ml glass vials with Teflon-lined screw-cap (Supelco Analytical) were filled
410 with 1.6 ml of melted 55°C -warm agarose solution, into which was dissolved 10 μl of pure
411 toluene. The toluene density is 0.87 g mL^{-1} and its molecular mass is 92.14 g mol^{-1} ; therefore,
412 adding 10 μl toluene to 1.6 ml volume is equivalent to 8.7 mg per 1.6 ml = 5.4 mg mL^{-1} . This
413 corresponds to 60 mM. This toluene stock was serially diluted in prewarmed agarose by
414 adding and mixing 0.15 ml of the agarose with the pure toluene source into 1.4 ml of 55°C -
415 warm agarose solutions, and from there to further agarose solutions. The 10^{-3} dilution is thus
416 equivalent to 60 μM . Toluene stocks were prepared fresh for every experiment.

417 Sources of benzoate were prepared by 100-fold dilution of a 1 M sodium benzoate
418 stock in 1.8 % 55°C -warm agarose, which corresponds to a concentration of 10 mM benzoate.

419 From here, benzoate was serially diluted in 55°C-warm agarose to obtain stocks of 1 and 0.1
420 mM. All vials were kept tightly closed in a water bath at 55°C until preparing the chambers.
421 Agarose solutions were prepared fresh for every experiment.

422 For ISCA assays, the chemoattractants were diluted in motility buffer without
423 agarose.

424 **Chemoattraction assays using agarose plugs on microscope slides.** While washing
425 the cell cultures, the microscope source chambers were prepared (Fig. S1). Chambers
426 consisted of a standard microscopy glass slide (Menzel Gläser, Thermo Scientific), onto
427 which two small coverslips (24×24 mm, 0.13-0.17 mm thick, MGF-Slides) were deposited on
428 both sides and maintained in place with ~10 µl of tap water. A drop of 4 µl of 55°C agarose
429 solution with the chemoattractant source (see above) was deposited in the middle and
430 immediately covered by a cleaned large coverslip (24×50 mm, Menzel Gläser) that bridges
431 over the side coverslips and thus creates a chamber with a height of 0.17 mm.

432 A freshly grown and washed bacterial suspension in motility buffer was inserted
433 around the agarose plug by pipetting 150 µl of cell suspension between the glass slide and the
434 large coverslip. *E. coli* standard assays with serine and other known chemoattractants were
435 carried out in triplicate in independent chambers. Toluene and benzoate assays were repeated
436 in fourfold replicates (one prepared *E. coli* culture, four independent chambers) in
437 conjunction with positive (serine) and negative (no attractant added) controls. Toluene assays
438 were further repeated on at least four independent occasions.

439 Bacterial accumulation was imaged after 15 min incubation at room temperature
440 (20±2 °C) using a DFC 350 FX R2 Leica camera mounted on an inverted DMI 4000 Leica
441 microscope using a N PLAN 10× objective. This timing was based on parallel video-imaging
442 of agarose source assays with a Dino-Lite digital microscope at 50× magnification (AnMo
443 Electronics Corporation, Taiwan) (Video S1). For each replicate, one image was taken at each
444 side of the agarose plug. Images were analyzed with ImageJ software (v. 1.49r,
445 <http://imagej.nih.gov/ij>). Cells were identified using the “find edges” routine in ImageJ and
446 the accumulated intensity values were quantified per zones of 25 pixels width (corresponding

447 to 2.5 μm) parallel to the plug border (3 zones in the plug and 27 zones outside the plug, Fig.
448 S1). Chemotactic responses were then averaged from four replicates. Intensity values were
449 summed and averaged across the three zones closest to the source edge, and intensity
450 variations among chemoattractants were analyzed in one-way ANOVA statistics.

451 ***In situ* chemotaxis assay (ISCA).** As an alternative, independent approach to the
452 agarose plug assays, we measured chemotaxis in the ISCA assay (21). An ISCA device
453 consists of a polydimethylsiloxane (PDMS) structure bonded to a glass slide, forming five
454 replicate circular wells, each having a volume of $\sim 110 \mu\text{l}$ that connects to the outside through
455 an acentrically placed, 0.8-mm diameter inlet port. Wells were filled through the inlet port
456 with a chemoattractant solution to the top, with care to leave a small (5 μl) droplet on the
457 surface of the inlet. The ISCA was then placed in a Petri dish, which was very slowly filled
458 with 55 ml of a suspension of *E. coli* at a density of $2\text{--}4 \times 10^6$ cells ml^{-1} (in motility buffer,
459 preheated at 37°C), until the ISCA was completely submerged. After 35 min of incubation at
460 room temperature (22°C), the external cell suspension was removed by pipetting and the
461 ISCA surface was wiped with a clean tissue. The contents of each ISCA well were collected
462 with a 1 ml syringe and a clean needle, transferred to a 200- μl well of a flat-bottom 96-well
463 culture plate, and mixed with 1 μl of a 1:100 dilution of SYBR Green I for cell staining.
464 Stained cell suspensions were kept on ice until all samples were obtained and then aspirated
465 into a Becton Dickinson Flow Cytometer, operated at $30 \mu\text{l min}^{-1}$ and counted over 60 sec.
466 From the cell counts (number of cells μl^{-1}) determined by flow cytometry for each ISCA
467 well, we computed the mean and the standard deviation across the five replicate wells.
468 Results presented in Fig. 4 were then obtained by normalizing to the mean cell count obtained
469 with the ISCA for the same strain on the same day over five replicate wells containing only
470 motility buffer (no-chemoattractant control), to quantify the enhancement in cell
471 concentration due to chemotaxis ('Normalized accumulation').

472 **Epifluorescence microscopy of fusion proteins.** In order to visualize the localisation
473 of McpT-, Tsr- and PcaY-mCherry expressed in *E. coli* MG1655, strains were precultured
474 with the same protocol as for the agarose plug assays. However, cells were resuspended in 50

475 μl of motility buffer after the final washing step. A drop of 7 μl of this cell suspension was
476 spotted on a 1% (*w/v*) agarose (in motility buffer) coated microscopy slide (layer thickness 1
477 mm) and then covered with a regular 0.17-mm thick glass coverslip. Cells were imaged at an
478 exposure time of 50 ms (phase-contrast) or 750 ms (mCherry) with a Nikon Eclipse Ti-E
479 inverted microscope, equipped with an ORCA-flash4.0 camera (Hamamatsu) and a Plan Apo
480 λ 100 \times 1.45 oil objective (Nikon). Images were recorded in ImageJ, saved as 8-bit grayscale
481 for reproduction, opened and cropped to their final size in Adobe Photoshop (v. CC2017), and
482 finally saved as .TIF with 300 dpi resolution for display. Cells were automatically segmented
483 using SuperSegger and standard *E. coli* parameter settings (35), and both cellular fluorescence
484 as well as the fluorescence intensities, scores and positions of up to 9 foci in individual cells
485 were extracted. Foci surpassing a focus score of 9 were listed using an in-house MatLab script
486 (version 2016a) and their positions were normalized to a standardized *E. coli* cell for
487 accumulated display. For expression quantification, cells with outlier mean fluorescence
488 levels (<5% and >95% percentiles) were removed, after which the top-10% pixel intensities
489 per cell were extracted (assuming this would correspond to the mCherry fusion protein
490 positions in foci or fluorescent bands) and averaged per cell, and further normalized by the
491 cell's mean fluorescence. This list of normalized average top 10% pixels per cell was then
492 multiplied by the average of all mean individual cellular fluorescence values for that strain
493 and incubation, in order to allow for inter-strain expression comparisons. Lists were randomly
494 subsampled in ten individual replicates, the means of which were used for ANOVA
495 comparison among strains, followed by Tukey's post hoc testing of statistical significance,
496 using the program *R*.

497

498 **ACKNOWLEDGMENTS**

499 We thank Vitali Maffenbeier for his help in cloning the PcaY-mCherry fusion construct. This
500 work was supported by the Swiss National Science Foundation NanoTera project 20NA21-
501 143082, by financing from the Herbette Foundation (2018-1-D-26), and by a grant from the
502 Gordon and Betty Moore Foundation (grant #3801 to RS). The authors declare no conflict of

503 interest. We thank the Stocker Lab at the ETH Zürich for advice and training in the ISCA

504 assay.

505

506 REFERENCES

- 507 1. Matilla MA, Krell T. 2017. Chemoreceptor-based signal sensing. *Curr Opin*
508 *Biotechnol* 45:8-14. <https://doi.org/10.1016/j.copbio.2016.11.021>.
- 509 2. Roggo C, van der Meer JR. 2017. Miniaturized and integrated whole cell living
510 bacterial sensors in field applicable autonomous devices. *Curr Opin Biotechnol*
511 45:24-33. <https://doi.org/10.1016/j.copbio.2016.11.023>.
- 512 3. Roggo C, Picioreanu C, Richard X, Mazza C, van Lintel H, van der Meer JR. 2018.
513 Quantitative chemical biosensing by bacterial chemotaxis in microfluidic chips.
514 *Environ Microbiol* 20:241-258. <https://doi.org/10.1111/1462-2920.13982>.
- 515 4. Sourjik V, Wingreen NS. 2012. Responding to chemical gradients: bacterial
516 chemotaxis. *Curr Opin Cell Biol* 24:262-268.
517 <https://doi.org/10.1016/j.ceb.2011.11.008>.
- 518 5. Sourjik V, Armitage JP. 2010. Spatial organization in bacterial chemotaxis. *EMBO J*
519 29:2724-2733. <https://doi.org/10.1038/emboj.2010.178>.
- 520 6. Alexander RP, Zhulin IB. 2007. Evolutionary genomics reveals conserved structural
521 determinants of signaling and adaptation in microbial chemoreceptors. *Proc Natl*
522 *Acad Sci U S A* 104:2885-2890. <https://doi.org/10.1073/pnas.0609359104>.
- 523 7. Lacal J, Garcia-Fontana C, Munoz-Martinez F, Ramos JL, Krell T. 2010. Sensing of
524 environmental signals: classification of chemoreceptors according to the size of their
525 ligand binding regions. *Environ Microbiol* 12:2873-2884.
526 <https://doi.org/10.1111/j.1462-2920.2010.02325.x>.
- 527 8. Szurmant H, Ordal GW. 2004. Diversity in chemotaxis mechanisms among the
528 bacteria and archaea. *Microbiol Mol Biol Rev* 68:301-319.
529 <https://doi.org/10.1128/MMBR.68.2.301-319.2004>.
- 530 9. Hazelbauer GL, Falke JJ, Parkinson JS. 2008. Bacterial chemoreceptors: high-
531 performance signaling in networked arrays. *Trends Biochem Sci* 33:9-19.
- 532 10. Sampedro I, Parales RE, Krell T, Hill JE. 2015. *Pseudomonas* chemotaxis. *FEMS*
533 *Microbiol Rev* 39:17-46. <https://doi.org/10.1111/1574-6976.12081>.
- 534 11. Baraquet C, Theraulaz L, Iobbi-Nivol C, Mejean V, Jourlin-Castelli C. 2009.
535 Unexpected chemoreceptors mediate energy taxis towards electron acceptors in
536 *Shewanella oneidensis*. *Mol Microbiol* 73:278-290. <https://doi.org/10.1111/j.1365-2958.2009.06770.x>.
- 537 12. Watts KJ, Taylor BL, Johnson MS. 2011. PAS/poly-HAMP signalling in Aer-2, a
538 soluble haem-based sensor. *Mol Microbiol* 79:686-699.
539 <https://doi.org/10.1111/j.1365-2958.2010.07477.x>.
- 540 13. Seitz MKH, Soto D, Studdert CA. 2012. A chemoreceptor from *Pseudomonas putida*
541 forms active signalling complexes in *Escherichia coli*. *Microbiology-Sgm* 158:2283-
542 2292. <https://doi.org/10.1099/mic.0.059899-0>.
- 543 14. Parales RE, Harwood CS. 2002. Bacterial chemotaxis to pollutants and plant-derived
544 aromatic molecules. *Curr Opin Microbiol* 5:266-273.
- 545 15. Krell T, Lacal J, Reyes-Darias JA, Jimenez-Sanchez C, Sungthong R, Ortega-Calvo
546 JJ. 2013. Bioavailability of pollutants and chemotaxis. *Curr Opin Biotechnol* 24:451-
547 456. <https://doi.org/10.1016/j.copbio.2012.08.011>.
- 548 16. Pandey G, Jain RK. 2002. Bacterial chemotaxis toward environmental pollutants: role
549 in bioremediation. *Appl Environ Microbiol* 68:5789-5795.
- 550 17. Parales RE, Luu RA, Hughes JG, Ditty JL. 2015. Bacterial chemotaxis to xenobiotic
551 chemicals and naturally-occurring analogs. *Curr Opin Biotechnol* 33:318-326.
552 <https://doi.org/10.1016/j.copbio.2015.03.017>.
- 553 18. Molina L, Duque E, Gomez MJ, Krell T, Lacal J, Garcia-Puente A, Garcia V, Matilla
554 MA, Ramos JL, Segura A. 2011. The pGRT1 plasmid of *Pseudomonas putida* DOT-
555 T1E encodes functions relevant for survival under harsh conditions in the
556 environment. *Environ Microbiol* 13:2315-2327. <https://doi.org/10.1111/j.1462-2920.2011.02492.x>.
- 557
558

- 559 19. Lacal J, Munoz-Martinez F, Reyes-Darias JA, Duque E, Matilla M, Segura A, Calvo
560 JJ, Jimenez-Sanchez C, Krell T, Ramos JL. 2011. Bacterial chemotaxis towards
561 aromatic hydrocarbons in *Pseudomonas*. Environ Microbiol 13:1733-1744.
562 <https://doi.org/10.1111/j.1462-2920.2011.02493.x>.
- 563 20. Luu RA, Kootstra JD, Nesteryuk V, Brunton CN, Parales JV, Ditty JL, Parales RE.
564 2015. Integration of chemotaxis, transport and catabolism in *Pseudomonas putida* and
565 identification of the aromatic acid chemoreceptor PcaY. Mol Microbiol 96:134-147.
566 <https://doi.org/10.1111/mmi.12929>.
- 567 21. Lambert BS, Raina JB, Fernandez VI, Rinke C, Siboni N, Rubino F, Hugenholtz P,
568 Tyson GW, Seymour JR, Stocker R. 2017. A microfluidics-based in situ chemotaxis
569 assay to study the behaviour of aquatic microbial communities. Nat Microbiol
570 2:1344-1349. <https://doi.org/10.1038/s41564-017-0010-9>.
- 571 22. Yu HS, Alam M. 1997. An agarose-in-plug bridge method to study chemotaxis in the
572 Archaeon *Halobacterium salinarum*. FEMS Microbiol Lett 156:265-269.
- 573 23. Keil H, Keil S, Pickup RW, Williams PA. 1985. Evolutionary conservation of genes
574 coding for meta pathway enzymes within TOL plasmids pWW0 and pWW53. J
575 Bacteriol 164:887-895.
- 576 24. Alper H, Fischer C, Nevoigt E, Stephanopoulos G. 2005. Tuning genetic control
577 through promoter engineering. Proc Natl Acad Sci U S A 102:12678-12683.
- 578 25. Hollands K, Lee DJ, Lloyd GS, Busby SJ. 2010. Activation of sigma 28-dependent
579 transcription in *Escherichia coli* by the cyclic AMP receptor protein requires an
580 unusual promoter organization. Mol Microbiol 75:1098-1111.
581 <https://doi.org/10.1111/j.1365-2958.2009.06913.x>.
- 582 26. Ping L, Weiner B, Kleckner N. 2008. Tsr-GFP accumulates linearly with time at cell
583 poles, and can be used to differentiate 'old' versus 'new' poles, in *Escherichia coli*.
584 Mol Microbiol 69:1427-1438. <https://doi.org/10.1111/j.1365-2958.2008.06372.x>.
- 585 27. Shiomi D, Banno S, Homma M, Kawagishi I. 2005. Stabilization of polar localization
586 of a chemoreceptor via its covalent modifications and its communication with a
587 different chemoreceptor. J Bacteriol 187:7647-7654.
588 <https://doi.org/10.1128/JB.187.22.7647-7654.2005>.
- 589 28. Pinas GE, DeSantis MD, Parkinson JS. 2018. Noncritical Signaling Role of a Kinase-
590 Receptor Interaction Surface in the Escherichia coli Chemosensory Core Complex. J
591 Mol Biol 430:1051-1064. <https://doi.org/10.1016/j.jmb.2018.02.004>.
- 592 29. Kihara M, Macnab RM. 1981. Cytoplasmic pH mediates pH taxis and weak-acid
593 repellent taxis of bacteria. J Bacteriol 145:1209-1221.
- 594 30. Bi S, Pollard AM, Yang Y, Jin F, Sourjik V. 2016. Engineering hybrid chemotaxis
595 receptors in bacteria. ACS Synth Biol 5:989-1001.
596 <https://doi.org/10.1021/acssynbio.6b00053>.
- 597 31. Derr P, Boder E, Goulian M. 2006. Changing the specificity of a bacterial
598 chemoreceptor. J Mol Biol 355:923-932. <https://doi.org/10.1016/j.jmb.2005.11.025>.
- 599 32. Miyazaki R, Minoia M, Pradervand N, Sulser S, Reinhard F, van der Meer JR. 2012.
600 Cellular variability of RpoS expression underlies subpopulation activation of an
601 integrative and conjugative element. PLoS Genet 8:e1002818.
602 <https://doi.org/10.1371/journal.pgen.1002818>.
- 603 33. Gerhardt P, Murray RGE. 1981. Manual of methods for general bacteriology.
604 American Society for Microbiology, Washington, D.C.
- 605 34. Berg HC, Brown DA. 1974. Chemotaxis in *Escherichia coli* analyzed by three-
606 dimensional tracking. Antibiot Chemother (1971) 19:55-78.
- 607 35. Stylianidou S, Brennan C, Nissen SB, Kuwada NJ, Wiggins PA. 2016. SuperSegger:
608 robust image segmentation, analysis and lineage tracking of bacterial cells. Mol
609 Microbiol 102:690-700. <https://doi.org/10.1111/mmi.13486>.
- 610 36. Gibson DT, Zylstra GJ, Chauhan S. 1990. Biotransformations catalyzed by toluene
611 dioxygenase from *Pseudomonas putida* F1, p 121-133. In Silver S, Chakrabarty AM,
612 Iglewski B, Kaplan S (ed), *Pseudomonas*: biotransformations, pathogenesis and
613 evolving biotechnology. American Society for Microbiology, Washington.

614

615

616 **TABLE 1** Used strains in this study

Strain lab collection n°	Host	Plasmid	Relevant characteristics	Source or reference
88	<i>P. putida</i> F1		Used as source for <i>pcaY</i>	(36)
1127	<i>P. putida</i> MT53	pWW53	Used as source for <i>mcpT</i>	(23)
3396	<i>E. coli</i> DH5 α	pBAM-link- mcherry	peptide-linker- <i>mcherry</i> coding sequence	(32)
4498	<i>E. coli</i> MG1655		Verified for motility	<i>E. coli</i> Genetic Center, Yale (CGSC#8237)
5396	<i>E. coli</i> Δ <i>tsr</i>		MG1655-derivative in which the <i>tsr</i> gene was deleted	This study
5186	<i>E. coli</i> DH5 α	pGEM-t- Easy- <i>trgp</i> - <i>mcp</i>	Amplified and cloned <i>trg</i> promoter from MG1655 plus first 12 bp of <i>mcpT</i>	This study
5197	<i>E. coli</i> MG1655	pCRO20	<i>trgp-mcpT</i> in pSTV28	This study
5447	<i>E. coli</i> MG1655	pCRO33	<i>trgp-pcaY</i> in pSTV28	This study
5448	<i>E. coli</i> MG1655	pCRO34	<i>trgp-tsr</i> in pSTV28	This study
5457	<i>E. coli</i> MG1655	pSTV28	cloning vector	Takara, Japan
5775	<i>E. coli</i> MG1655	pCRO35	<i>trgp-mcpT_{FS}</i> in pSTV28, frameshift mutation in <i>mcpT</i> coding sequence	This study
5782	<i>E. coli</i> MG1655	pCRO36	<i>trgp-mcpT-mcherry</i> fusion on pSTV28	This study
5839	<i>E. coli</i> MG1655	pCRO37	as pCRO36, but with a frameshift mutation in <i>mcpT</i>	This study
5841	<i>E. coli</i> MG1655	pCRO38	<i>trgp-tsr-mcherry</i> fusion on pSTV28	This study
5924	<i>E. coli</i> MG1655	pCRO33- mChe	<i>trgp-pcaY-mcherry</i> fusion on pSTV28	This study
6085	<i>E. coli</i> Δ <i>tsr</i>	pCRO20	Strain 5396 carrying <i>trgp-mcpT</i>	This study
6068	<i>E. coli</i> Δ <i>tsr</i>	pCRO33	Strain 5396 carrying <i>trgp-pcaY</i>	This study
5846	<i>E. coli</i> Δ <i>tsr</i>	pCRO36	Strain 5396 carrying <i>trgp-mcpT</i> - <i>mcherry</i>	This study
6010	<i>E. coli</i> Δ <i>tsr</i>	pCRO33- mChe	Strain 5396 carrying <i>trgp-pcaY</i> - <i>mcherry</i>	This study
6013	<i>E. coli</i> Δ <i>tsr</i>	pCRO38	Strain 5396 carrying <i>trgp-tsr</i> - <i>mcherry</i>	This study

617

618

619

620 **FIG 1** Chemotaxis response of *E. coli* MG1655 towards various common attractants in
621 agarose plug assays. (A) Average cell accumulation of *E. coli* MG1655 as a function of
622 distance from the source edge with 100 μ M of serine, aspartate, methylaspartate, ribose,
623 galactose or a no attractant control. Ribbon traces show the average of triplicates (central line)
624 \pm one standard deviation (bordering lines). (B) as (A) but with source concentration of 10 μ M
625 of the different attractants. (C) Average gray values across the three zones closest to the
626 source edge (7.5 μ m width) summarized for the different attractants and concentrations.
627 Asterisks indicate significantly different values at $p < 0.0001$ in one-way ANOVA followed by
628 Tukey post-hoc multiple comparison test.

629

630

631 **FIG 2** Chemotaxis of *E. coli* expressing *mcpT* of *P. putida* towards toluene. (A) Cropped
632 100-fold magnification phase-contrast images of one agarose plug replicate experiment with
633 sources containing no attractant (Ctl), 60 μ M toluene (Tol) or 100 μ M serine (Ser). Yellow
634 curves represent the measured cell accumulation. Note the agarose sources localized on the
635 left of the images with the source edge typically resulting in a dark-light band. (B) Average
636 cell accumulation (as image average grey values, AGV) as a function of distance from the
637 source edge averaged from four biological replicates imaged on both sides of the agarose plug
638 with toluene (0.6 mM and 60 μ M), serine (100 μ M) or a no-added attractant control for *E.*
639 *coli* MG1566 (pCRO20) expressing the McpT receptor from *P. putida* MT53. Ribbon traces
640 show the average of four replicates \pm one standard deviation. Inset shows the average grey
641 value across the three zones closest to the source edge (7.5 μ m width). Letters indicate
642 significance groups in a one-way ANOVA followed by post-hoc Tukey multiple comparison
643 test. (C) As (B) but with *E. coli* MG1655 (pSTV) (empty plasmid). (D) As (B) but with *E.*
644 *coli* MG1655 (pCRO35), which contains a frameshift mutation in *mcpT* causing premature
645 translation stop.

646

647

648

649 **FIG 3** Chemotaxis response of PcaY expressing *E. coli* MG1655. (A) Cell accumulation as a
650 function of distance to an agarose plug with benzoate (1 or 0.1 mM), serine (100 μ M) or no
651 attractant of *E. coli* MG1566 (pCRO33) expressing the PcaY receptor for benzoate of *P.*
652 *putida* F1. (B) As (A) for *E. coli* MG1566 (pSTV) (empty plasmid). Cell accumulation,
653 ribbon traces and inset as in the legend to Figure 2. Benzoate source concentration is 1 mM
654 for the data shown in the inset.

655

656

657 **FIG 4** *E. coli* cell accumulation in wells of an *in-situ* chemotaxis microfabricated chip. (A) *E.*
658 *coli* MG1655 wild-type (strain 4498), (B) *E. coli* MG1655 (pCRO20) expressing McpT
659 (strain 5197), (C) *E. coli* MG1655 (pCRO33) expressing PcaY (strain 5447), (D) *E. coli*
660 MG1655- Δ *tsr* (pCRO33) expressing PcaY (strain 6068), (E) *E. coli* MG1655- Δ *tsr* (pCRO20)
661 expressing McpT (strain 6085). Bars show average cell accumulation plus SD (error bars) to
662 the indicated chemoattractants measured by absolute flow cytometric counting across five-
663 fold replicate cavities, normalized to that of cavities filled with motility buffer (MB) alone.
664 Note that panels may be composed of different independent experiments, which are
665 normalized to the respective cell accumulation in MB as control for every individual
666 chemotaxis assay. SER, serine; BEN, benzoate; TOL, toluene. Concentrations in μ M or mM,
667 as indicated. Asterisks and sword-signs denote significantly increased and decreased
668 responses, respectively, compared to motility buffer at p-values < 0.05 in pair-wise t-tests.

669

670

671 **FIG 5** Characterization of MCP receptor expression in *E. coli* by fluorescent protein fusions.
672 Phase contrast (PhC) and mCherry (mCHE) epifluorescence images of, respectively, (A), *E.*
673 *coli* MG1655 (pCRO34), expressing the Tsr receptor (TSR), (B) MG1655 (pCRO38),
674 expressing a Tsr-mCherry fusion protein (TSR-MCHERRY), (C) MG1655 (pCRO36),

675 expressing a fusion protein of McpT and mCherry (MCPT-MCHERRY), (D) MG1655
676 (pCRO37), expressing an mCherry fusion protein but with a frameshift mutation in *mcpT*
677 coding sequence (MCPT^{FS}-MCHERRY), (E) MG1655 (pCRO20) expressing McpT (MCPT),
678 and (F), MG1655 (pCRO33-mCHE), expressing the PcaY-mCherry fusion protein. Arrows in
679 panels C and F show visible membrane foci of McpT-mCherry and PcaY-mCherry. Images
680 were recorded and auto-scaled in ImageJ, saved as 8-bit grayscale for reproduction, opened
681 and cropped to their final size in Adobe Photoshop (v. CC2017), and finally saved as .TIF
682 with 300 dpi resolution for display. Numbers in fluorescence images indicate the absolute
683 intensity scaling (min–max) for reproduction.

684

685 **FIG 6** Localization and quantification of chemoreceptor-mCherry fluorescent protein fusions
686 in *E. coli*. (A) Positions of fluorescent foci (black dots) in *n* individual cells extracted by
687 SuperSegger from image series in the different strains (as indicated), superposed and plotted
688 on a standardized *E. coli* cell by a MatLab custom subroutine. (B) Heatmap of fluorescent
689 pixel intensity extracted from 1000 *E. coli* cells showing the position of Tsr-mCherry
690 fluorescence normalized to a standardized cell length and width. (C) Average top–10% pixel
691 intensity per cell among *n* cells as from panels A-H, normalized to the mean fluorescence
692 intensity of all cells of that strain. Error bars show SD of 10 images. Note the different
693 intensity scales between strains expressing McpT derivatives, PcaY-mCherry and Tsr-
694 mCherry. Letters above bars indicate statistically significantly different categories in
695 ANOVA, followed by Tukey post-hoc testing ($p < 0.005$).

696

697 **SUPPLEMENTAL MATERIAL**

698

699 **Figure S1: Agarose source cell accumulation assay.** (A) Setup of the microscope chamber,
700 the position of the agarose disk and insertion of the cell suspension. (B) Cell accumulation
701 quantification. Phase contrast images of the border of the agarose plug were taken with the
702 10x objective of an inverted phase-contrast microscope. A copy of the image is produced
703 using the “find edges” routine of ImageJ. A segmented line following the border of the
704 agarose plug is drawn *manually* in ImageJ. The line is *enlarged* to 25 pixels width that creates
705 a band, which was moved and copied in order to obtain three zones inside the plug (in red)
706 and 27 zones at successive contacting distances from the source edge (in orange). The average
707 gray value intensity was then quantified for each band.

708

709 **Figure S2. Plasmid constructs used in this study.** All plasmids were produced in the
710 pSTV28 backbone. Relevant restriction sites for cloning are indicated. The reading frames of
711 *mcpT*, *pcaY*, *tsr* and *mCherry* are depicted as colored bars, whereas the *trg* promoter region
712 (P_{trg}) is depicted as a brown bar with an upright bended arrow.

713

714 **Figure S3. Relevant sequence details of cloned MCP genes.** (A) Relevant sequence detail
715 of the cloned *mcpT* gene in pCRO20. (B) Relevant sequence detail of the cloned *pcaY* gene in
716 pCRO33. (C) Relevant sequence detail of the *mcpT-mCherry* fusion in pCRO36.

717

718 **Figure S4. Cobalt Clustall alignment of the type 40H *P. putida* MCPs (McpT, PcaY and**
719 **PctA) and the *E. coli* Tsr and Tar type 36H.** Functional assignment of MCP regions
720 (helices N22-N01 and C01-C22) corresponding to the classification of Alexander et al (6).
721 Residues in Red: *E. coli* pentapeptide motif is NWETF, binding CheR and CheB, but
722 expanded by structural studies and preliminary sequence analysis to the motif -x-[HFWY]-
723 x(2)-[HFWY]-, allowing any aromatic residue in the second and fifth positions (6). Residues
724 in rose: Predicted methylation site motifs in the methylation subdomain (heptads 13–22).

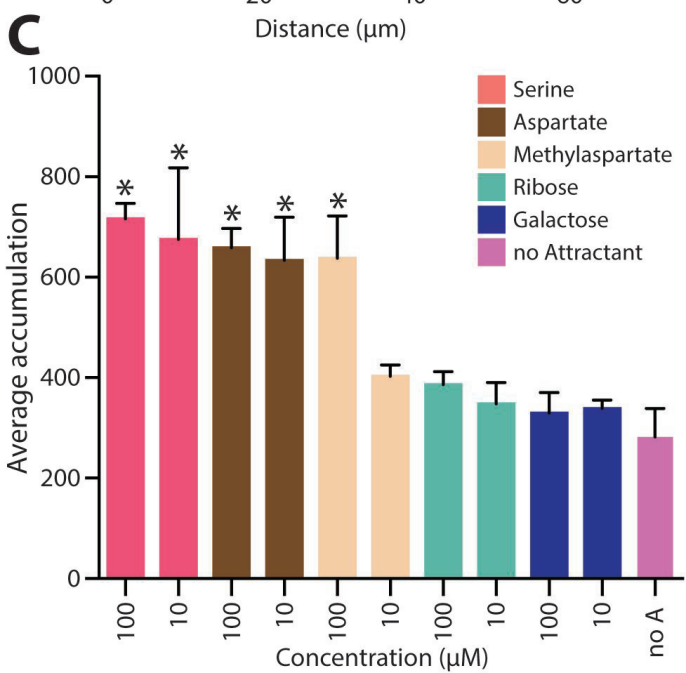
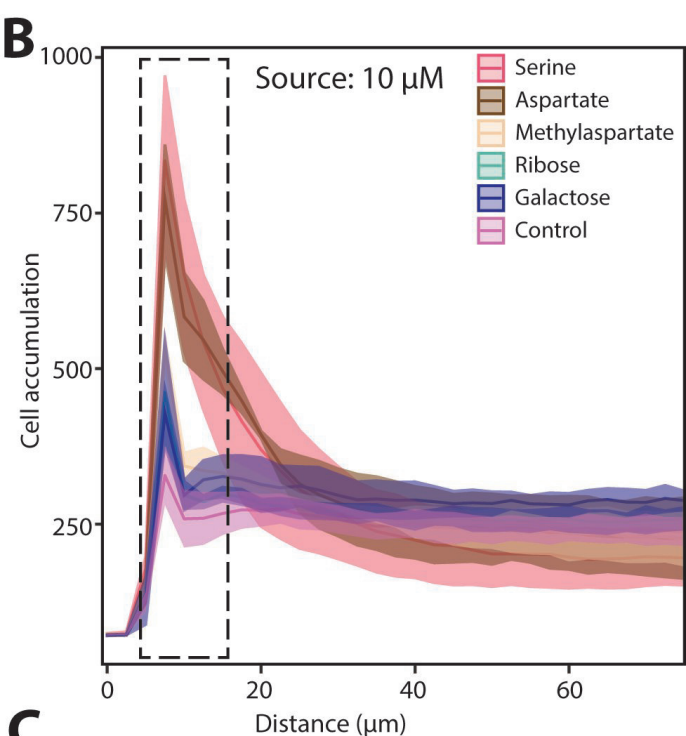
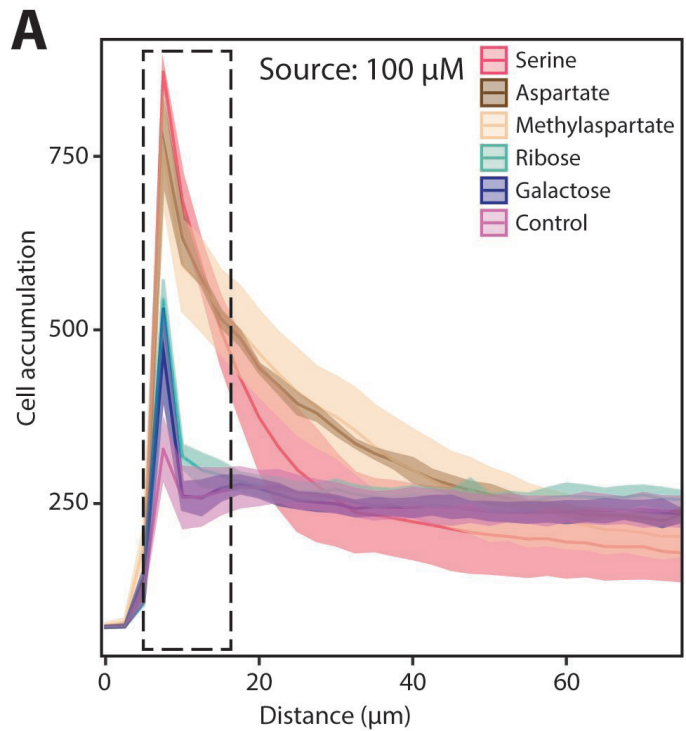
725 Consensus methylation sequence for the MCP_CD family according to (6): -[ASTG]-
726 [ASTG]-x(2)-[EQ]-[EQ]-x(2)-[ASTG]-[ASTG]-. Residues in blue: R388 and V398 of Tsr
727 that have been shown to contact CheW (6). Residues in brown: Reported CheA-P5 cleft
728 contacts to Tsr (N-helix residues F373, N376, L380, A383, V384, A387, and G390)(28).
729 Symbols: *, conserved amino acids across all five MCPs. ^, inter- and intra-dimer sites (6). In
730 36H-class receptors (Tsr) the Phe-residue stabilizes the trimer of dimers.

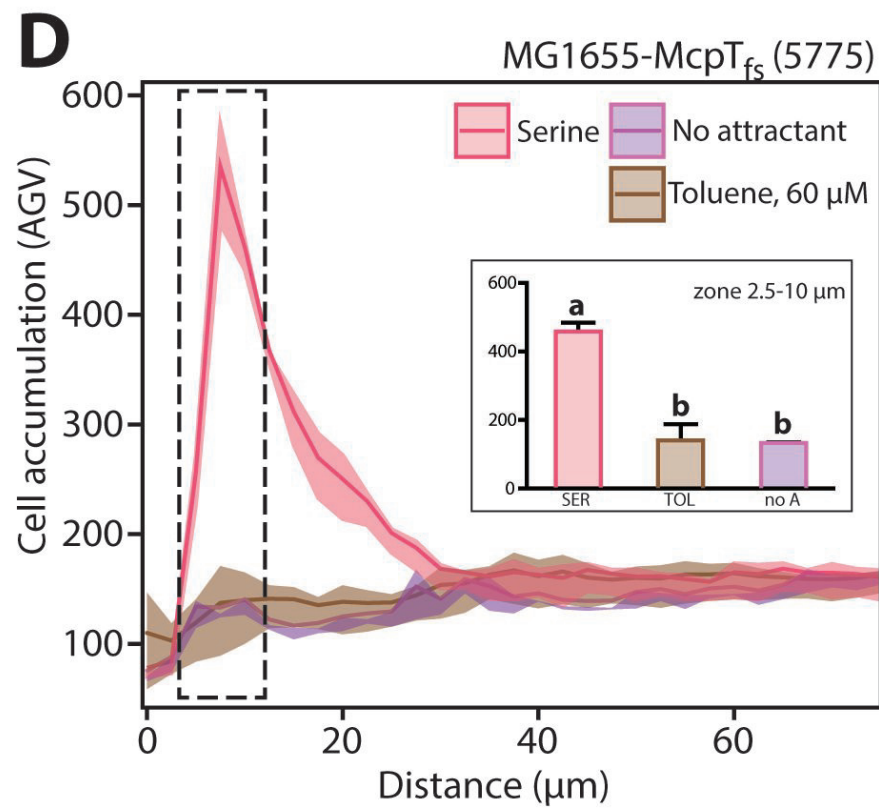
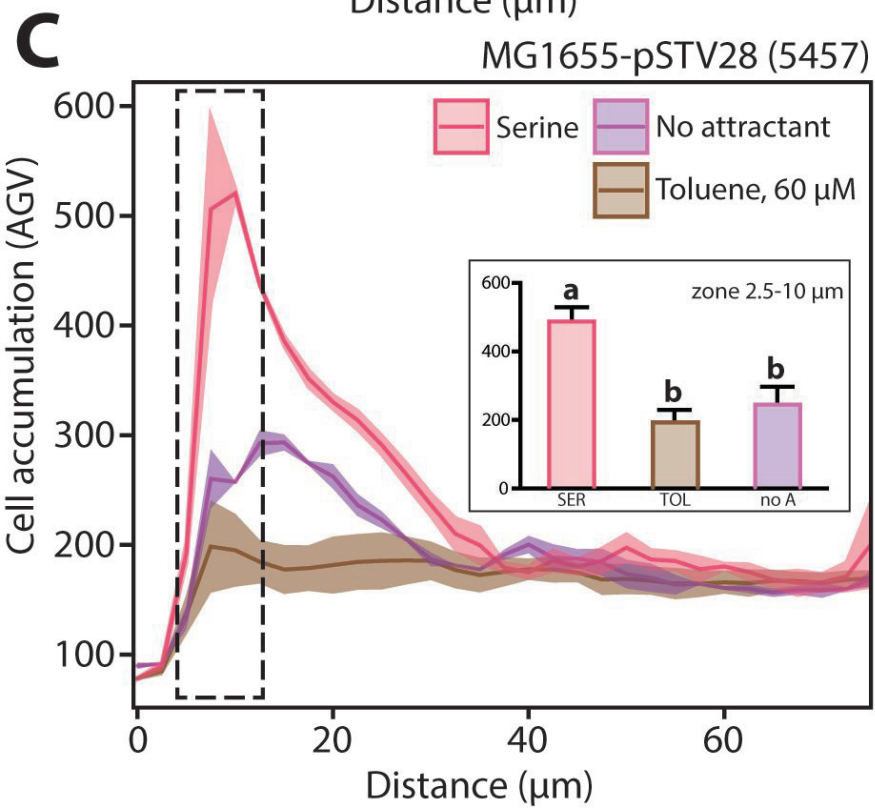
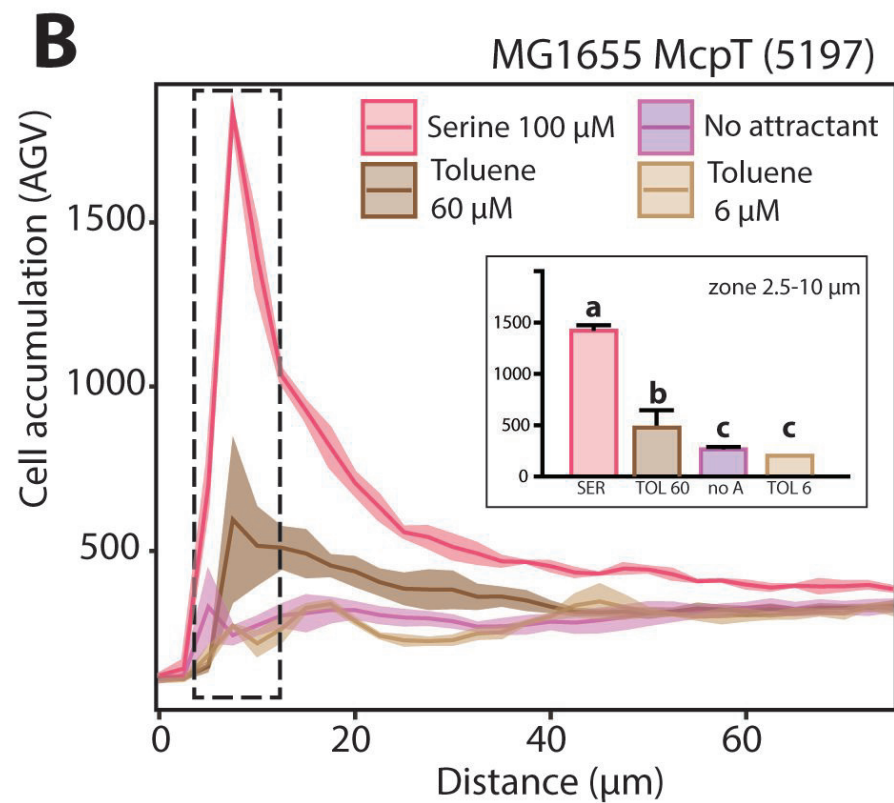
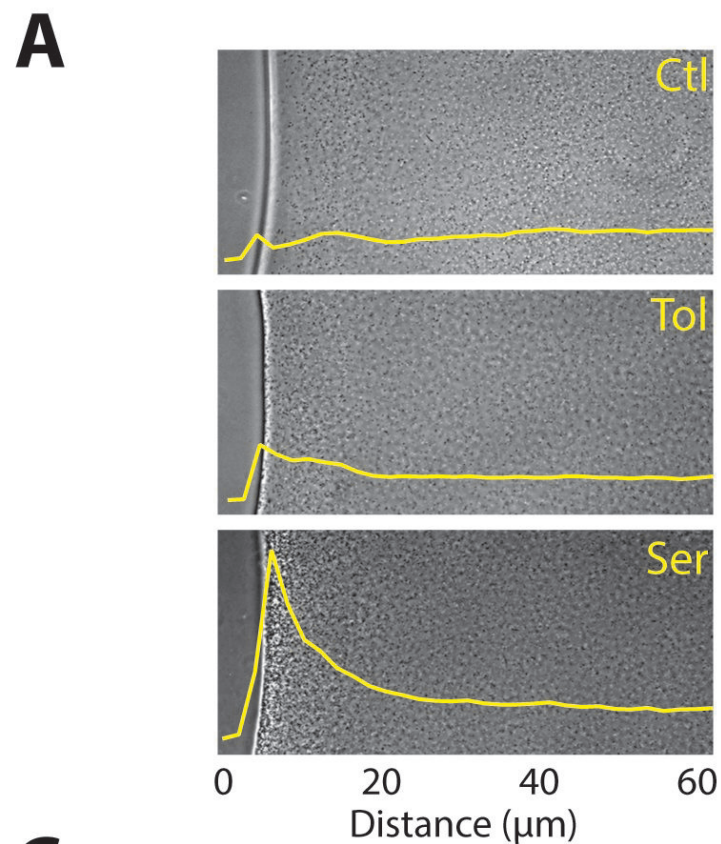
731

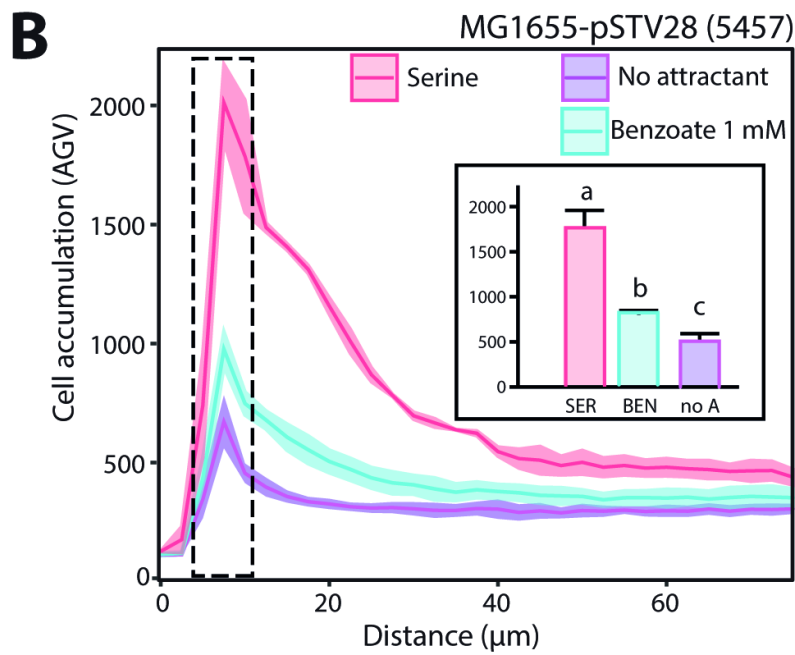
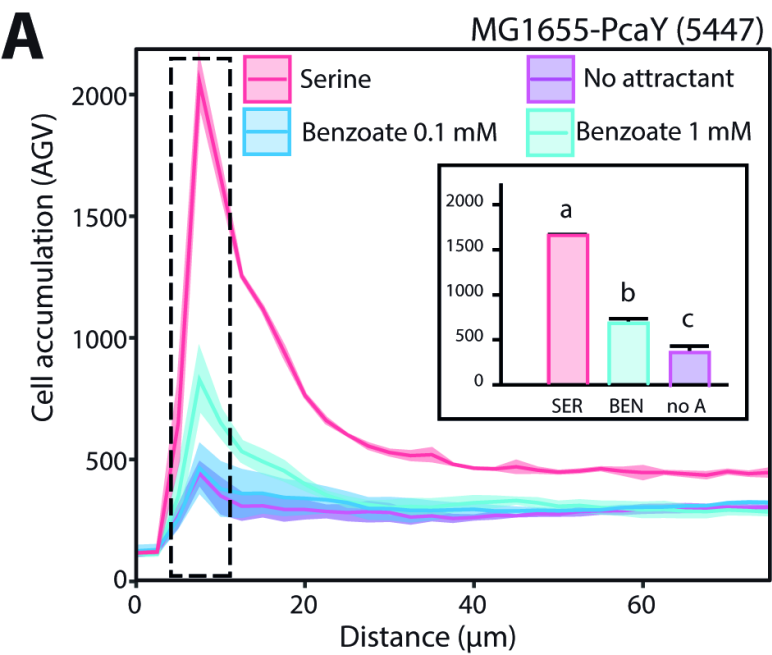
732 **Table S1. Primers used in this study.**

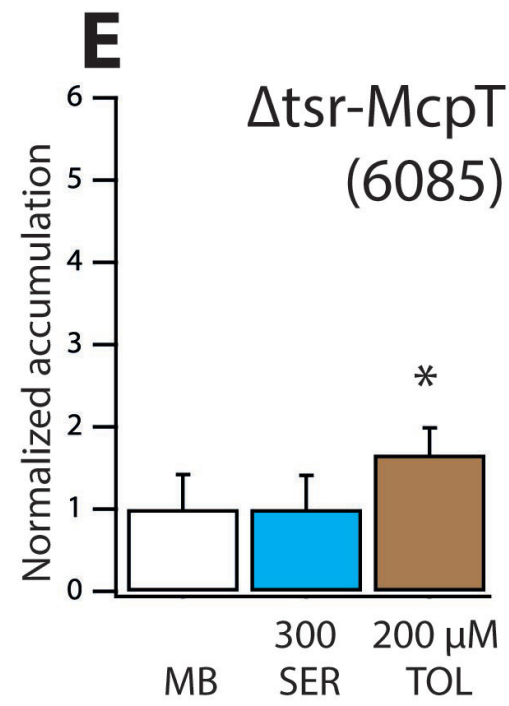
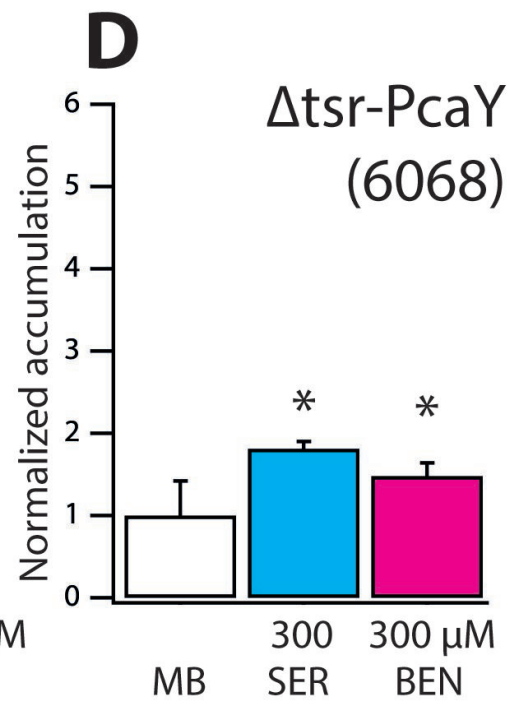
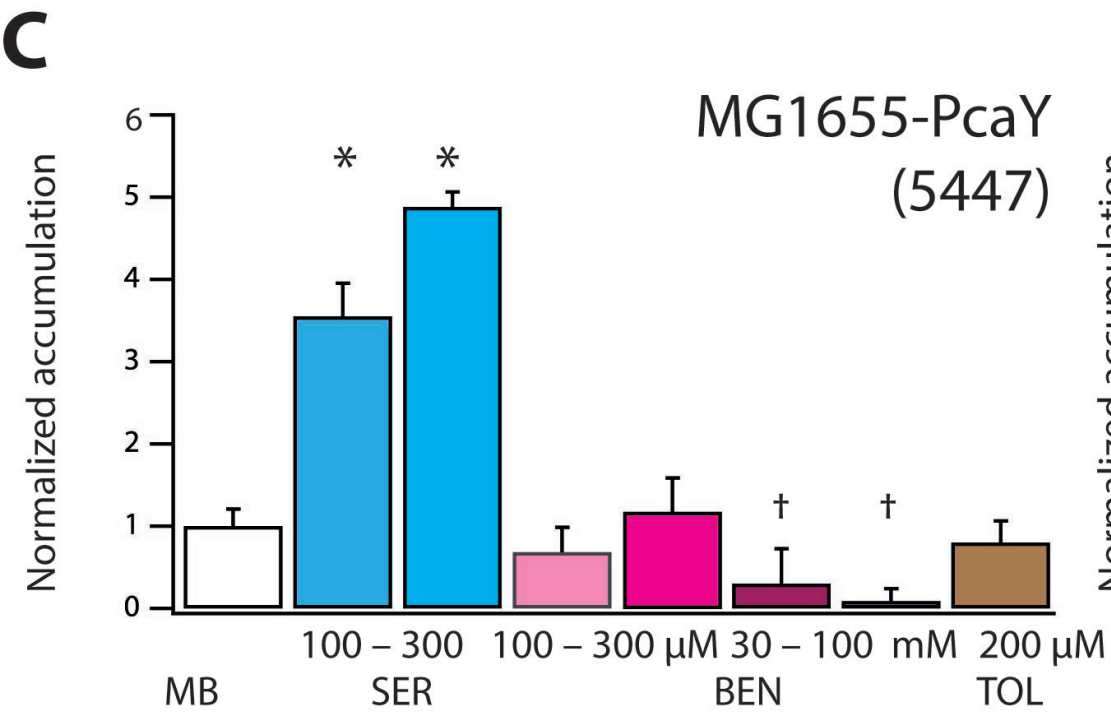
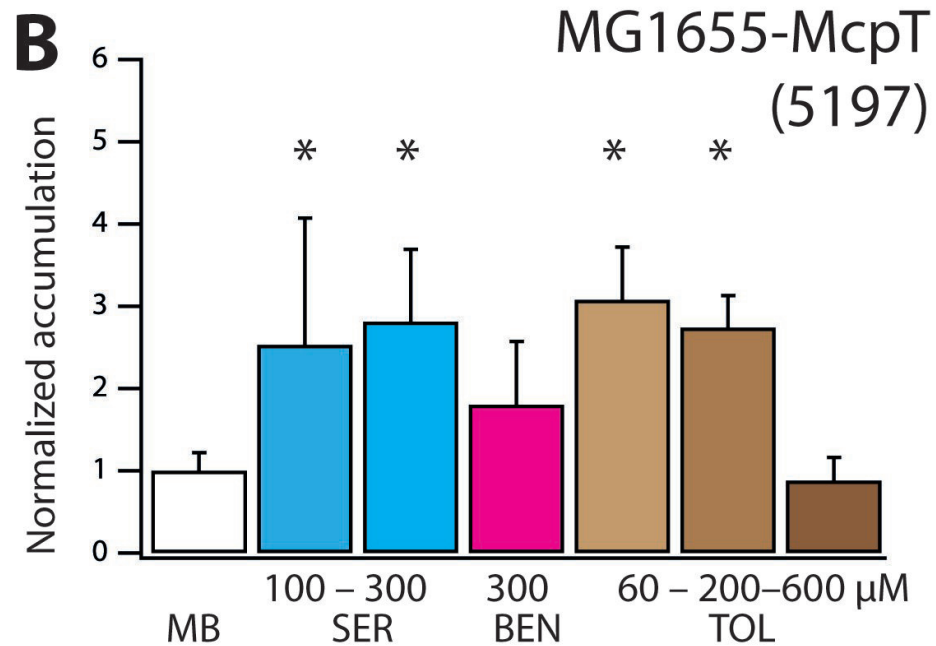
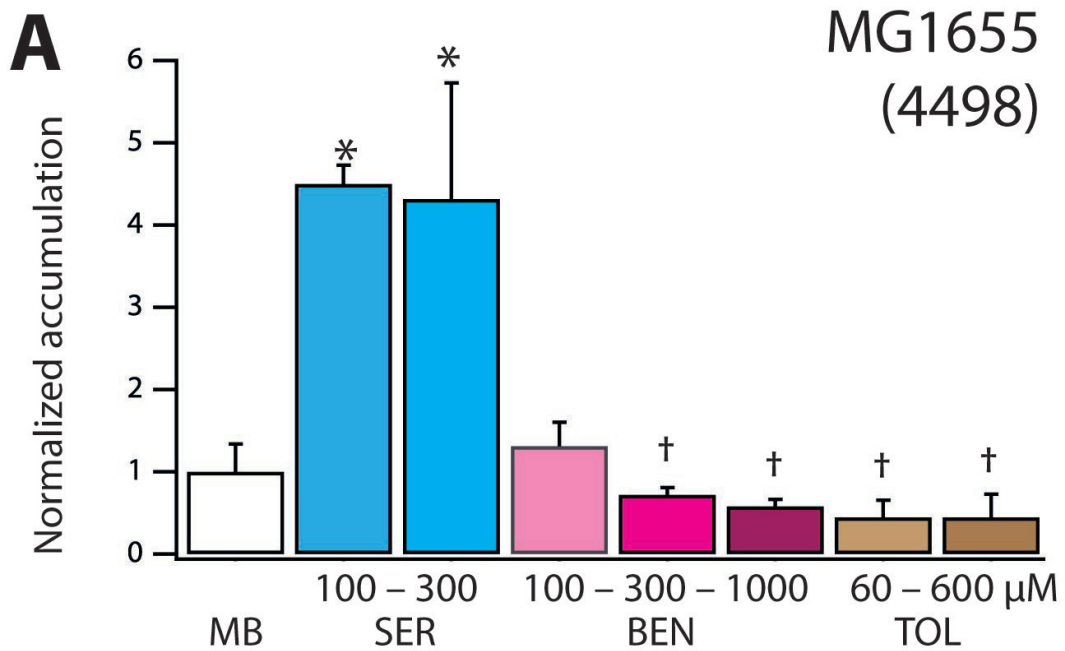
733

734

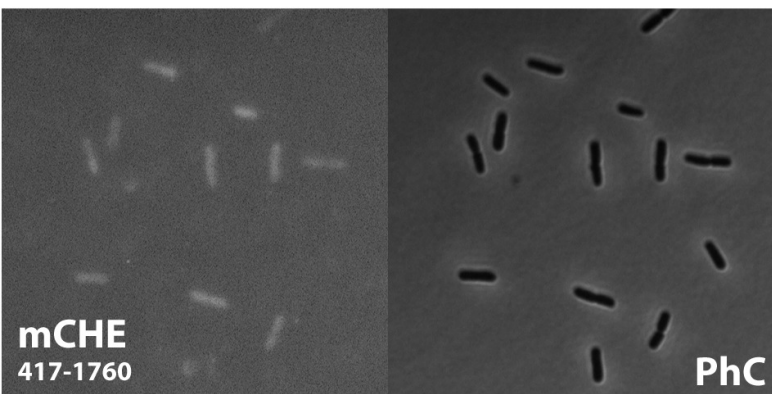




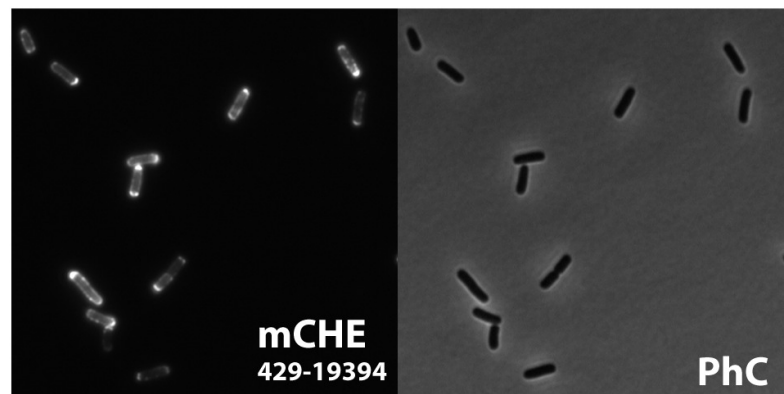




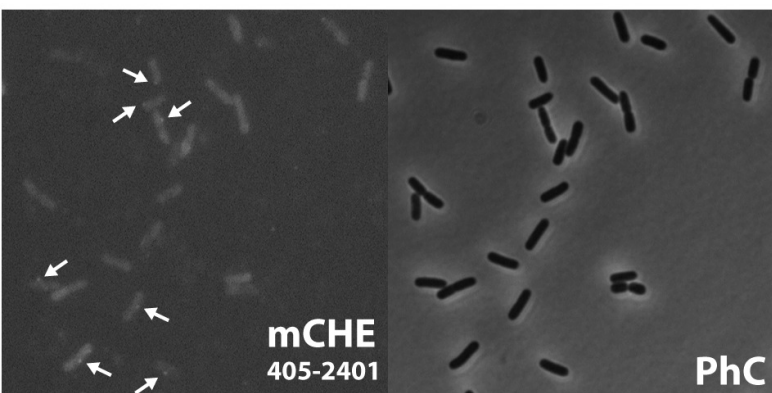
A 5448 TSR



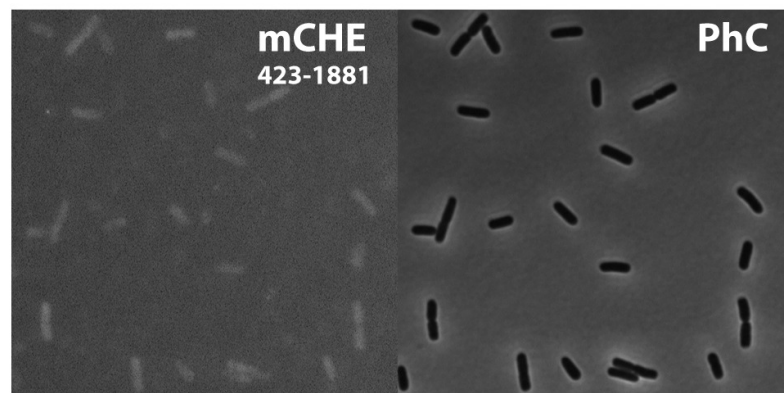
B 5841 TSR-MCHERRY



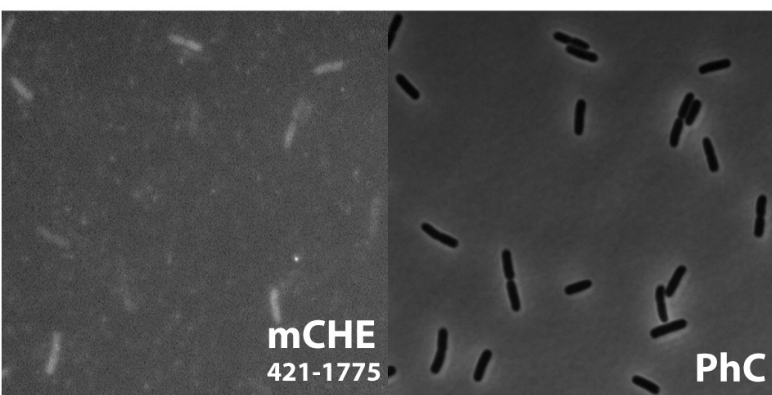
C 5782 MCPT-MCHERRY



D 5839 MCPT^{FS}-MCHERRY



E 5197 MCPT



F 5924 PcaY-MCHERRY

